Theory and hierarchical calculations of the structure and energetics of [0001] tilt grain boundaries in graphene

Johan M. Carlsson,[1,2,*] Luca M. Ghiringhelli,[2] and Annalisa Fasolino[3]

[1]*Accelrys Ltd, Cambridge Science Park 334, Cambridge CB4 OWN, United Kingdom*

[2]*Fritz-Haber-Institut der Max-Planck-Gesellschaft, Faradayweg 4-6, DE-14195 Berlin, Germany*

[3]*Institute for Molecules and Materials, Radboud University Nijmegen, Heyendaalseweg 135, NL-6525 AJ Nijmegen, The Netherlands*

(Received 5 May 2011; published 11 October 2011)

Several experiments have revealed the presence of grain boundaries in graphene that may change its electronic and elastic properties. Here, we present a general theory for the structure of [0001] tilt grain boundaries in graphene based on the coincidence site lattice (CSL) theory. We show that the CSL theory uniquely classifies the grain boundaries in terms of the misorientation angle θ and periodicity d using two grain-boundary indices (m,n), similar to the nanotube indices. The structure and formation energy of a large set of grain boundaries generated by the CSL theory for $0^\circ < \theta < 60^\circ$ (up to 15 608 atoms) were optimized by a hierarchical methodology and validated by density functional calculations. We find that low-energy grain boundaries in graphene can be identified as dislocation arrays. The dislocations form hillocks like those observed by scanning tunneling microscopy in graphene grown on Ir(111) for small θ that flatten out at larger misorientation angles. We find that, in contrast to three-dimensional materials, the strain created by the grain boundary can be released via out-of-plane distortions that lead to an effective attractive interaction between dislocation cores. Therefore, the dependence on θ of the formation energy parallels that of the out-of-plane distortions, with a secondary minimum at $\theta = 32.2^\circ$ where the grain boundary is made of a flat zigzag array of only 5 and 7 rings. For $\theta > 32.2^\circ$, other nonhexagonal rings are also possible. We discuss the importance of these findings for the interpretation of recent experimental results.

DOI: 10.1103/PhysRevB.84.165423 PACS number(s): 61.48.Gh, 61.72.Mm

I. INTRODUCTION

Graphene has extraordinary electronic,[1,2] structural,[3,4] and mechanical[5,6] properties, but utilizing these properties in applications requires the ability to grow large-scale graphene sheets. The groundbreaking method to exfoliate graphene sheets from graphite crystals[1] is, in general, found to provide perfect, defect-free graphene sheets over large length scales, but exfoliation is not suitable for large-scale production. Several other routes are currently pursued to synthesize graphene,[7–12] but the samples created in these ways are often found to be polycrystalline. For instance, recent transmission electron microscopy (TEM) investigations of graphene grown by chemical vapor deposition (CVD) have shown that these samples have an average grain size of 250 nm,[13] which is much smaller than the grain size in highly oriented pyrolytic graphite (HOPG) (6–30μm). The defects in these graphene samples can, on the one hand, be detrimental for the properties of graphene and, on the other hand, offer a potential mean to control its mechanical[14] and electronic[15,16] properties. Interestingly, recent scanning tunneling microscopy (STM) experiments have found that grain boundaries strongly influence the electronic properties in graphene by causing metallization along the boundary.[15]

Grain-boundary engineering at the atomic level is, however, still very challenging because the basic principles of the structure of grain boundaries in graphene are not well known. Investigations of grain boundaries in graphene and graphite have shown very different geometries depending on the position of the rotation axis and the misorientation angle between the grains on opposite sides of the boundary. Early STM investigations of [0001] tilt grain boundaries in HOPG with misorientation angles 6.5°, 8°, and 19° found these grain boundaries to have an amorphous structure.[17] More recent STM investigations of graphene grown on the Ir(111) surface show that small-angle [0001] tilt grain boundaries with misorientation angles around $\theta \approx 2^\circ$ have the shape of periodic arrays of asymmetric hillocks with a large separation of approximately 70 nm. The buckling is attributed to a pentagon-heptagon (5-7) ring complex that could be identified as a dislocation core.[18] Another STM investigation of a [0001] tilt grain boundary in HOPG with large misorientation angle ($\theta = 39^\circ$) could also be characterized as a flat array of 5-7 ring complexes, but with a much shorter periodicity of about 0.7 nm.[19] Recent STM investigations of multiple [0001] tilt grain boundaries in HOPG confirmed the trend that small-misorientation-angle grain boundaries form separated hillocks, which gradually merge into ridges and finally become flat for large misorientation angles.[20]

Also, other combinations of nonhexagonal rings have been reported and attributed to matching with the substrate. For instance, a large-angle [0001] tilt grain boundary with misorientation angle of $\theta = 60^\circ$ has been observed by STM for graphene grown on Ni(111) and identified as an array of 5-5-8 rings.[15] In summary, the experimental observations indicate that small-misorientation-angle [0001] tilt grain boundaries can be characterized as 5-7 dislocation arrays, as is often observed for grain boundaries in three-dimensional materials,[21] while large-misorientation-angle grain boundaries can have periodic patterns containing other combinations of nonhexagonal rings in agreement with the structural unit model.[22] It is desirable to have a general theory to predict the atomistic structure of grain boundaries in graphene capturing the variation from small to large misorientation angles. Several

theoretical works have studied the effect of selected grain boundaries on electronic structure and transport by either assuming the grain boundary as a dislocation array[14,23–26] or by combining arbitrarily cut edges into high-energy amorphous grain boundaries.[27,28]

We have developed such a general theory for the structure of [0001] tilt grain boundaries in graphene based on the coincidence site lattice (CSL) theory that is able to predict the low-energy structure of these grain boundaries, with the misorientation angle θ as the only input parameter. The theory is able to characterize the various grain boundaries that have been observed in experiments recently,[13,15,18–20] ranging from small to large misorientation angles.

In order to obtain a general understanding of [0001] tilt grain boundaries in graphene, we have used the CSL theory to construct a large set of grain boundaries in the whole range of misorientation angles. The grain-boundary structures are then studied by a hierarchical methodology: the constructed structures are optimized by force-field calculations using the Dreiding force field[29] as well as by the more accurate reactive bond-order potential LCBOPII.[30] The formation energies are then calculated by the LCBOPII potential, which gives results in very good agreement with those obtained by DFT calculations for selected structures. This systematic approach allows us to find general trends as a function of the misorientation angle and divide the formation energy into a core, a strain, and a core-core interaction term. In particular, the formation energy per dislocation cores is found to be closely correlated with the out-of-plane distortion, since they are both described by a V-shaped curve with a minimum at $\theta = 32.2^\circ$. This is characteristic of two-dimensional (2D) structures, where strain can be released by out-of-plane distortions.

In Sec. II, we present the CSL theory for the construction of grain boundaries; in Sec. III, we describe the procedure we have used to optimize the structures and calculate the formation energy; in Sec. IV, we present our results; finally, in Sec. V, we present a summary and conclusions.

II. CSL THEORY OF GRAIN BOUNDARIES IN THE TWO-DIMENSIONAL HEXAGONAL LATTICE

The geometrical structure of [0001] tilt grain boundaries in the hexagonal lattice of graphene can be derived using the CSL theory.[31] The basic assumption of the CSL theory is that the most energetically favorable grain boundaries provide the smoothest possible connection between two misoriented grains. These grain boundaries have an ordered, periodic structure and can be imagined to be the result of the following procedure, which is illustrated in Fig. 1. Two ideal lattices are superimposed and rotated by an angle θ with respect to each other around a given axis, a process that gives rise to a moiré pattern (the interference pattern that occurs between two superimposed lattices that are either reciprocally tilted or have slightly different mesh sizes). For specific misorientation angles, this pattern is characterized by the coincidence between points in the two lattices with a regular periodicity. These points form the coincidence site lattice. The grain boundary is then constructed by cutting the two superimposed lattices along a line through the coincidence lattice sites and joining the part of the upper lattice (black lattice in Fig. 1) above

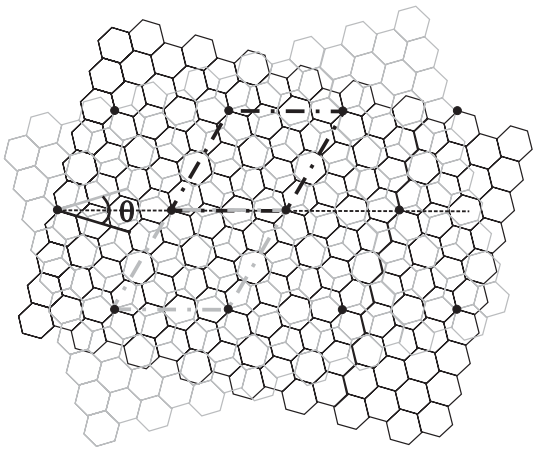

FIG. 1. Illustration of the coincidence site lattice (CSL) formed by rotating two hexagonal lattices with respect to each other by an angle $\theta = 32.2^\circ$ corresponding to the $\Sigma = 13$ grain boundary. The coincidence sites between the black and the white lattice that form the coincidence site lattice are highlighted by the black dots. The CSL cells for the black and white lattices, indicated by the dashed-dotted black and white rhombuses, are defined as the area of the respective lattices, which are limited by the coincidence sites. The cut plane through the CSL points is indicated by the thin dotted line.

the cut with the part of the bottom lattice (white lattice in Fig. 1) below the cut. This procedure gives rise to a grain boundary, where the separation of the coincident lattice points corresponds to the periodicity of the structural units along the grain boundary. The lattice sites that do not coincide in the two lattices are frustrated and will rearrange to minimize the energy as we will describe in Sec. III.

To generate a CSL grain boundary for graphene, we need to find those coincidence points in the hexagonal lattice that can be superimposed by a pure rotation. This is most easily done by taking symmetric points on either side of a mirror plane. Graphene has two families of mirror planes, the armchair line along the (1,1) direction and the zigzag line along the (0,1) direction. In order to find the CSL points, it is more convenient to use the armchair line as mirror plane, indicated in Fig. 2 by a dotted (horizontal) line, because it passes through the lattice points. The construction using the zigzag line (at 30° from the armchair line) would lead to equivalent structures, but it is more cumbersome because the line passes in-between the lattice points. Notice that the misorientation angles defined with respect to zigzag lines[14,19] θ_{zz} are related to the misorientation angles defined with respect to the armchair line used in this paper: $\theta_{ac} \equiv \theta$ by $\theta_{zz} = 60^\circ - \theta$. We call the lattice points above the mirror plane the black lattice and the lattice points below the mirror plane the white lattice. Some points of the two lattices are indicated in Fig. 2(a) by black and white dots.

The generating vector for the black lattice

$$\mathbf{R}_1^b = m\mathbf{a}_1 + n\mathbf{a}_2 \tag{1}$$

is identified by the two indices (m,n) referring to the lattice vectors in graphene $\mathbf{a}_{1,2} = (3a_0/2, \mp\sqrt{3}a_0/2)$, where $a_0 = 1.42$ Å is the interatomic distance in graphene. The *grain-boundary indices* (m,n) determine the structures of the grain

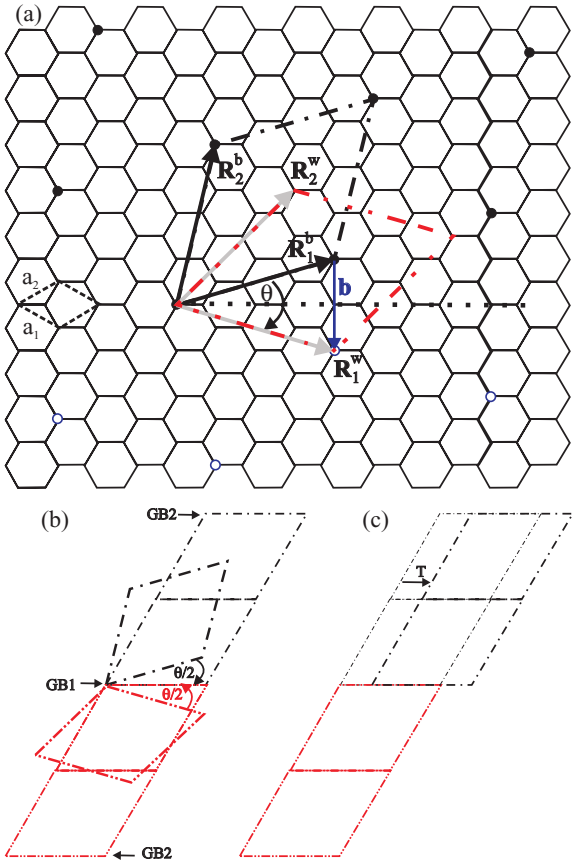

FIG. 2. (Color online) (a) How to identify the coincidence site lattice cells for a hexagonal lattice using the (1,1)-lattice direction as the mirror plane. The black CSL lattice points for $\Sigma = 13$ that has $(m,n) = (1,3)$ are indicated by the black dots and the lattice points in the white lattice by open circles. The generating vector $\mathbf{R}_1^b$ is shown by the black arrow, the Burger's vector $\mathbf{b}$ by the blue arrow, and the vector $\mathbf{R}_1^w$ by the gray arrow. The black and red dashed-dotted lines mark the CSL unit cell for the black and white lattices respectively. (b) Construction of the grain-boundary supercell. The black cell is rotated by $-\theta/2$ and the white cell is rotated by $\theta/2$. Two black cells and two white cells are then joined to form the supercell for the grain boundary. This supercell provides a periodic model that contains two grain boundaries GB1 and GB2. (c) The relative translation of the two grains is simulated by translating the black cells with respect to the white cells by a translation vector T that is a fraction of the period d of the grain boundary.

boundaries in analogy to the chiral indices of nanotubes. The lattice points that correspond to the generating vectors of the black lattice $\mathbf{R}_1^b$ are shown in Fig. 3(a).

The length of the generating vector gives the periodicity d:

$$d = |\mathbf{R}_1^b| = a\sqrt{m^2 + mn + n^2}, \tag{2}$$

where $a = \sqrt{3}a_0$ is the modulus of both $\mathbf{a}_1$ and $\mathbf{a}_2$. The CSL points for the white lattice on the opposite side of the mirror plane $\mathbf{R}_1^w$ are found by adding to $\mathbf{R}_1^b$ the Burger's vector $\mathbf{b}$:

$$\mathbf{b} = a(n-m)(1,-1) \tag{3}$$

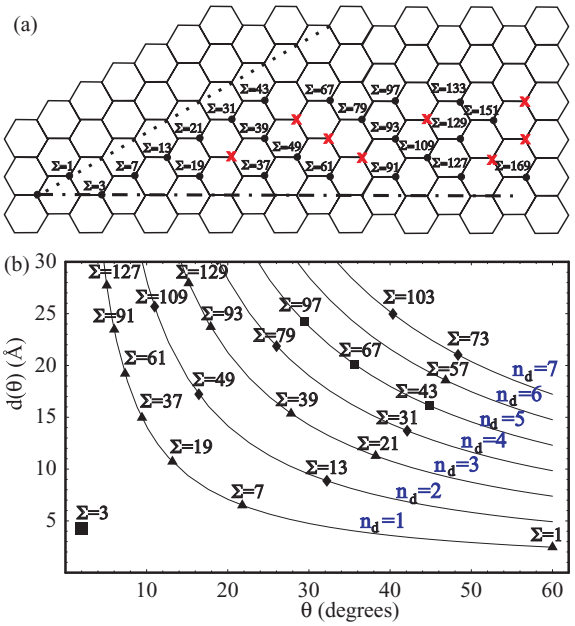

FIG. 3. (Color online) (a) The periodic table of generating vectors $\mathbf{R}_1^b$ for CSL grain boundaries in graphene indicated by black dots. The lattice points are denoted by the Σ values and the lattice points that correspond to an integer multiple of a shorter generating vector are indicated by red crosses. (b) The relationship between misorientation angle θ, the period of the grain boundary d, and the size of the CSL cell Σ. The lines are given by Frank's formula in Eq. (5) and connect CSL grain boundaries with the same Burger's vector into the grain-boundary families, characterized by n_d (see Secs. IV and IV B). The dots indicate the discrete values of θ that correspond to exact CSL grain boundaries and the Σ values are given by Eq. (9).

perpendicular to the armchair mirror plane as indicated in Fig. 2(a), giving

$$\mathbf{R}_1^w = \mathbf{R}_1^b + \mathbf{b} = a(n,m). \tag{4}$$

The misorientation angle θ between $\mathbf{R}_1^b$ and $\mathbf{R}_1^w$ is given by Frank's formula[31] and can be expressed in terms of the grain-boundary indices

$$\theta = 2\arcsin\left(\frac{|\mathbf{b}|}{2|\mathbf{R}_1^b|}\right) = 2\arcsin\left(\frac{|n-m|}{2\sqrt{m^2+mn+n^2}}\right). \tag{5}$$

The unit cell for the black CSL lattice is then determined by two vectors: by $\mathbf{R}_1^b$ and by the vector $\mathbf{R}_2^b$, which has the same length, but is rotated by 60° with respect to $\mathbf{R}_1^b$,

$$\mathbf{R}_2^b = a(-n,m+n). \tag{6}$$

The second vector that spans the white CSL cell $\mathbf{R}_2^w$ is similarly rotated by 60° with respect to $\mathbf{R}_1^w$:

$$\mathbf{R}_2^w = a(-m,m+n). \tag{7}$$

The size $\Omega_{\text{CSL cell}}$ of the CSL unit cell, normalized to the size $\Omega_{\text{unit cell}}$ of the unit cell of the underlying lattice, is denoted by Σ, and the Σ value is used to characterize the CSL grain

TABLE I. Summary of the parameters of the CSL theory for grain boundaries in graphene. The relaxed period length d_{rel} is in nm.

n	m	Σ	θ	d_{rel}	n_d
26	25	1951	1.3	10.85	1
16	15	721	2.1	6.576	1
10	9	271	3.5	4.039	1
15	13	589	4.7	5.953	2
7	6	127	5.1	2.759	1
11	9	301	6.6	4.252	2
5	4	61	7.3	1.912	1
9	7	193	8.3	3.405	2
13	10	399	8.6	4.905	3
4	3	37	9.4	1.489	1
7	5	109	11	2.562	2
10	7	219	11.6	3.632	3
3	2	19	13.2	1.068	1
8	5	129	15.2	2.787	3
5	3	49	16.4	1.716	2
7	4	93	17.9	2.366	3
9	5	151	18.7	3.018	4
2	1	7	21.8	0.652	1
7	3	79	26.0	2.183	4
5	2	39	27.8	1.531	3
8	3	97	29.4	2.420	5
3	1	13	32.2	0.888	2
4	1	21	38.2	1.123	3
5	1	31	42.1	1.363	4
7	1	57	46.8	1.846	6
2	0	4	60	0.655	1

boundaries. For graphene, Σ can be expressed in terms of the grain-boundary indices as

$$\Sigma = \frac{\Omega_{\text{CSL cell}}}{\Omega_{\text{unit cell}}} = m^2 + mn + n^2. \tag{8}$$

Considering that there are two atoms in the unit cell of graphene, a CSL unit cell contains 2Σ atoms. Finally, using Eqs. (2), (5), and (8) gives the nonlinear relation between θ and Σ:

$$\Sigma = \frac{\mathbf{b}^2}{\left[2a\sin\left(\frac{\theta}{2}\right)\right]^2}. \tag{9}$$

For easy reference, we have collected the grain-boundary indices (m,n) that are connected to the misorientation angle θ and the normalized area of the CSL cell Σ that we discuss in this article in Table I. Note that the period d_{relaxed} of the relaxed structure is only ~0.01–0.02 Å different from the theoretical value d [(Eq. (2)]. We have also generated a periodic table of lattice points that correspond to the generating vectors of the black lattice $\mathbf{R}_1^b$ in Fig. 3(a) and the dependence of the size Σ of the CSL cell on the misorientation angle θ and period d is shown in Fig. 3(b).

A supercell model for the grain boundary can be constructed by the following steps once the grain-boundary indices (m,n) of a CSL grain boundary that correspond most closely to the desired misorientation angle θ have been determined: starting from a lattice point, one has to identify which lattice points of the graphene lattice fall within the black CSL cell defined by the lattice vectors $\mathbf{R}_1^b$ and $\mathbf{R}_2^b$ as indicated in Fig. 2(a). Starting from the same lattice point, the same procedure is done for the white CSL cell formed by $\mathbf{R}_1^w$ and $\mathbf{R}_2^w$. The black CSL cell is rotated by $-\theta/2$, while the white CSL cell is rotated by $\theta/2$ in order to bring the edges of the CSL cells to coincide as shown in Fig. 2(b).

For calculations using periodic boundary conditions, it is convenient to construct a periodic structure by generating two antisymmetric grain boundaries per supercell, so that the periodicity of the lattice perpendicular to the grain boundaries is restored. In doing this, one has to take into account the strain interaction between the two grain boundaries in the periodic supercell. Elasticity theory predicts that the strain field perpendicular to the grain-boundary line decays exponentially with length scale d,[31] so that grain boundaries in the supercell need to be separated by at least a distance $2d$ to diminish the self-interaction. To this purpose, we insert four CSL cells (two white and two black cells) into a hexagonal supercell as shown schematically in Fig. 2(b). With this method to construct the supercell for a grain boundary defined by a certain Σ, the number of atoms in the supercell is 8Σ.

In addition, the two grains that meet at a grain boundary can slide with respect to each other, so that it is necessary to search for the optimal relative translation between the black and white CSL cells, as illustrated in Fig. 2(c). The optimal *translation state* corresponds to the relative translation that provides the structure of the grain boundary with the lowest formation energy.

The c direction of the supercell perpendicular to the graphene plane was set to 15 Å for DFT calculations to diminish the interaction between the graphene sheets in adjacent supercells. In the calculations with the LCBOPII, instead, we have kept a much larger value, to allow for out-of-plane distortions that can become large for very large samples.

The CSL theory was implemented in a script in Materials Studio[32] to generate a large set of supercell models that span the misorientation angle from 0° to 60°. A collection of the grain-boundary models is presented in Fig. 4 and will be discussed in Sec. IV. For practical reasons, we have used rectangular rather than hexagonal supercells. The largest supercell for the $\Sigma = 1951$ grain boundary contained 15 608 atoms. Finally, the generated grain-boundary supercells need to be geometry optimized with respect to atomic positions and supercell lattice parameters.

III. METHODS FOR ENERGY CALCULATION

The grain-boundary models generated by the CSL theory were geometry optimized by a hierarchical combination of three methods. The supercell models were initially optimized by atomistic force-field calculations using the Dreiding force field[29] as implemented in the FORCITE code in Materials Studio.[32] The optimization was performed until the forces were below 1 meV/Å, the variation in total energies was below 10^{-6} eV/atom, and the stress was below 1 MPa. The Dreiding force field provides a fast method for rough optimization of the atomic structures of the grain-boundary models. However, a more precise evaluation of the formation energy is provided by the reactive bond-order potential LCBOPII, which has been optimized to reproduce the elastic properties of carbon in a

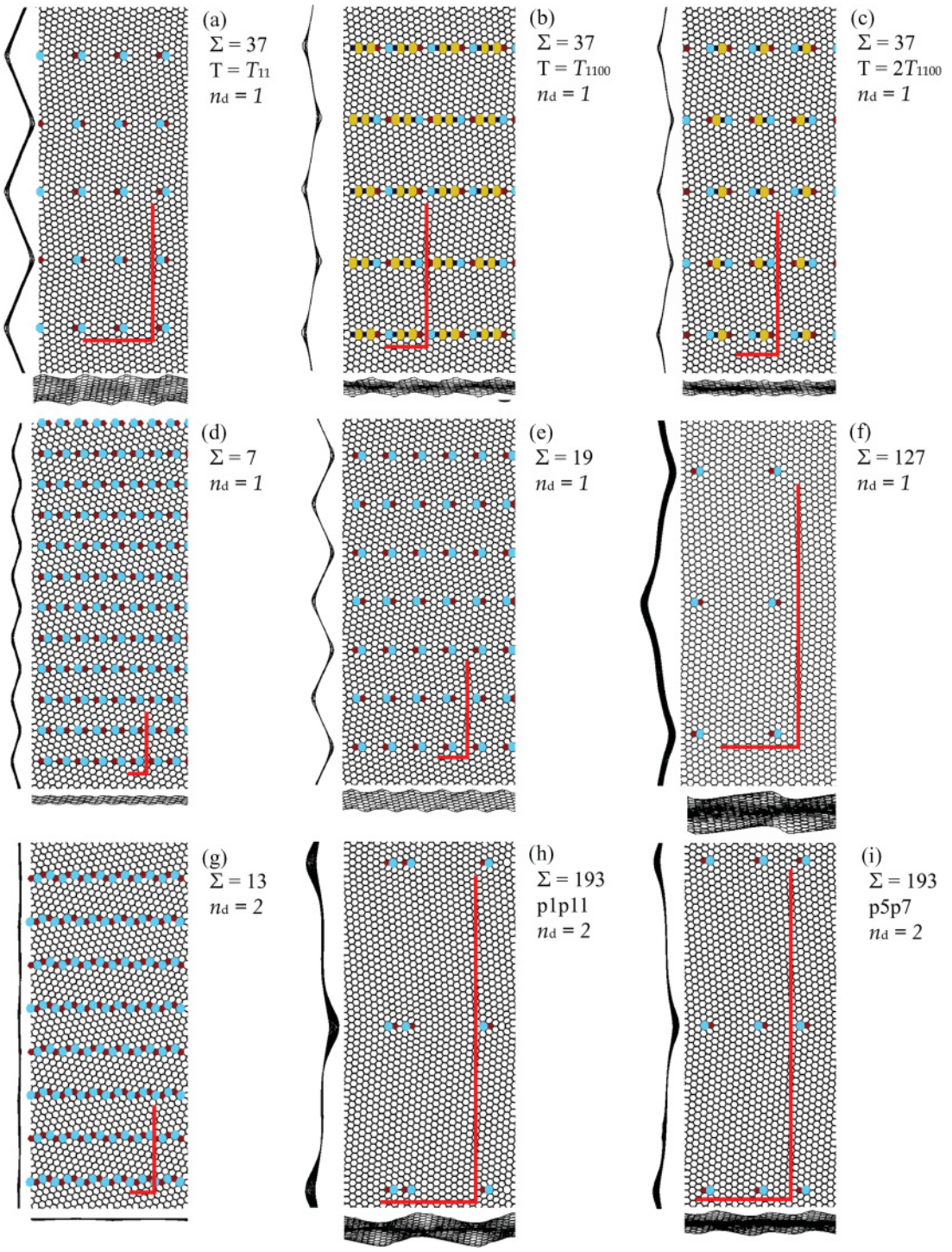

FIG. 4. (Color online) Atomic structures of various [0001] tilt grain boundaries in graphene (fully relaxed). The nonhexagonal rings are highlighted as follows: squares are purple, pentagons are red, heptagons are cyan, and octagons are yellow. The red lines mark the (rectangular) unit cell. All panels are at the same scale. (a)–(c) Three different translational states of the $\Sigma = 37$ grain boundary. (a) The lowest-energy translation state is an array of dislocation cores (5-7) rings. (b) The translation state contains a sequence of 7-4-8-4-8-5-6 rings. (c) The translation state contains a sequence of 5-8-4-7-6-6-6 rings. (d)–(f) The lowest-energy structures of the first family ($\mathbf{b} = a$) containing one dislocation core per period. (g)–(i) The lowest-energy structures of the second family ($\mathbf{b} = 2a$). (g) The structure of the $\Sigma = 13$ grain boundary that has the lowest formation energy of the large-misorientation-angle grain boundaries. Panels (h) and (i) show two different arrangements of the secondary dislocation arrays for the $\Sigma = 193$ grain boundary. The arrangement in (i) with the two dislocation arrays in close proximity has lower formation energy than the more equally spaced array in (h).

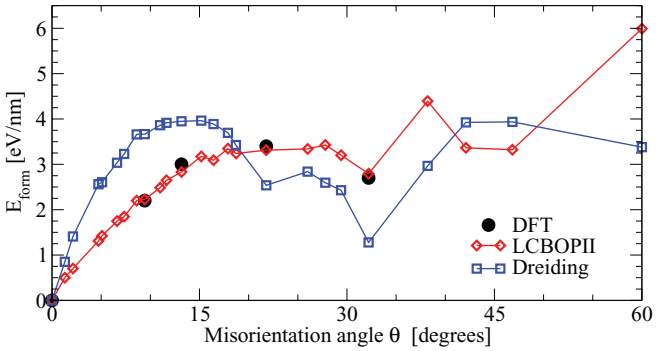

FIG. 5. (Color online) The formation energy per unit length of [0001] tilt grain boundaries in graphene as a function of misorientation angle θ calculated using three different methods: force-field calculations with the Dreiding force field (blue line), force-field calculations with the bond-order potential LCBOPII (red line), and DFT calculations with GGA-PBE exchange-correlation functional (black circles).

variety of configurations.[30] The structure relaxations with the LCBOPII were performed with a dedicated Monte Carlo code, through an annealing cycle. Namely, the Dreiding optimized structure was heated up in steps up to 700 K and then cooled in slower steps down to 10 K. The average energy at 10 K was then corrected for the $3/2Nk_BT$ potential energy given by equipartition, in order to yield the values reported in our plots. Figure 5 shows that formation energies calculated with the LCBOPII reproduce very accurately the DFT values, so that it is possible to obtain accurate formation energies for grain boundaries with significantly larger unit cells than those accessible by direct *ab initio* calculations. The *ab initio* calculations were based on the density functional theory (DFT) in the generalized gradient approximation (GGA),[33] as implemented in the CASTEP code.[34] The ultrasoft pseudopotential for carbon was optimized for a plane-wave energy cutoff of 450 eV. The supercell contained up to 296 atoms (for the $\Sigma = 37$ grain boundary). The grain-boundary geometries were optimized until the atomic forces were less than 0.01 eV/Å and the stress in the cell was less than 10 MPa.

The formation energy of the grain boundary is calculated as

$$E^{\mathrm{GB}}_{\mathrm{form}}(\theta) = \frac{E^{\mathrm{GB}}(\theta,n_{\mathrm{C}}) - n_{\mathrm{C}}\mu_{\mathrm{C}}}{2d}, \tag{10}$$

where E^{GB} is the total energy of the supercell containing the grain boundary model with n_{C} C atoms, μ_{C} is the chemical potential of graphene (−7.349 eV according to LCBOPII, fitted to the experimental value, and −7.774 eV according to PBE-DFT), and d is the periodicity of the grain boundary.

IV. RESULTS

A. Translation states

The first step to determine the atomic structure of the grain-boundary region for a particular misorientation angle θ is to analyze the translation states. In Figs. 4(a)–4(c), we show, for the particular case of $\Sigma = 37$, that a variety of nonhexagonal rings, such as 4, 5, 7, and 8 rings, can appear due to the lattice mismatch and the actual combination depends on the relative translation between the two lattices. These nonhexagonal rings cause an energy cost, although the carbon atoms are always threefold coordinated in the low-energy structures of symmetric tilt grain boundaries in contrast to the grain boundaries investigated in Ref. 27.

The formation energy of the structure shown in Fig. 4(a), with only one pair of 5-7 rings, is 2.23 eV/nm, whereas the formation energy for the other two structures of Figs. 4(b) and 4(c) are 6.32 and 4.62 eV/nm, respectively. We have found that, for all studied grain boundaries with $\theta \leqslant 32.2^\circ$, the lowest-energy structures contain only 5-7 pairs. These 5-7 pairs can be identified as an edge dislocation core in the hexagonal lattice as the heptagon requires an additional line of atoms on one side compared to the hexagons, and the pentagon closes the bonds between the atoms in the additional line of atoms and the adjacent atoms in the hexagonal lattice. Therefore, the low-energy structures for small-misorientation-angle grain boundaries in graphene can, in general, be characterized as dislocation arrays in agreement with STM observations of grain boundaries in graphene[18] and graphite.[19] This result provides a theoretical basis for the recent theoretical articles that have modeled the grain boundaries as dislocation arrays.[14,23–26] For misorientation angles larger than 32.2°, however, the low-energy grain boundaries can also contain other nonhexagonal rings than 5-7 pairs. In particular, for $(m,n) = (0,2)$ with $\Sigma = 4$ and $\theta = 60^\circ$, the low-energy structure contains at the grain boundary 8-rings separated by two adjacent 5-rings exactly as observed for graphene on Ni(111).[15] Also, this structure results naturally from the CSL theory.

B. Interaction between the dislocation cores in the grain boundary

Further analysis of our grain-boundary models reveals that the atomic structure of the grain-boundary region can more generally be described as an array of n_{rings} per period given by

$$n_{\mathrm{rings}} = m + n. \tag{11}$$

The number of nonhexagonal rings in this array is given by the number of dislocation cores needed to provide the misorientation angle. The number of dislocation cores per period n_d in turn depends on the length of the Burger's vector in units of the modulus a of the lattice vectors $\mathbf{a}_1$ and $\mathbf{a}_2$, which may be expressed by the grain-boundary indices

$$n_d = |\mathbf{b}|/a = |n - m|. \tag{12}$$

Hence, the number of nonhexagonal rings $n_{n\neq 6}$ is given by $2n_d$, since each dislocation core introduces a 5-7 pair of rings:

$$n_{n\neq 6} = 2n_d = 2|n - m|. \tag{13}$$

The grain boundaries may now be divided into families based on the number of dislocation cores per period n_d as shown in Fig. 3(b). The primary family with $n_d = 1$ has one dislocation core per period of the grain boundary, so the separation of the dislocation cores is equal to the period d as can be seen in Figs. 4(d)–4(f). The families with $n_d > 1$, instead, contain more than one dislocation core per period as can be seen in Figs. 4(g)–4(i). The secondary dislocation arrays

have the same periodicity as the primary dislocation array, but they are translated with respect to the primary dislocation array. The distance between the primary and secondary dislocation arrays depends on the interaction between the dislocation cores and is not fixed by the CSL theory. Therefore, it is a free parameter that has to be optimized.

The interaction between the dislocation cores in three-dimensional materials is usually repulsive, so that a secondary dislocation array provides an additional energy cost.[31] This would imply that grain boundaries with $\theta \neq \theta_{n_d=1}$ would have a formation energy higher than the grain boundary in the family $n_d = 1$. We will show in the following that, in graphene, the dislocation cores attract each other.

To determine how the dislocation cores interact in a two-dimensional material, such as graphene, we have studied in detail the $n_d = 2$ family, which contains one secondary dislocation array. To describe the different configurations of primary and secondary dislocation lines, we use the notation of a sequence of p for the 5-7 pair, followed by a number that indicates how many hexagons separate the dislocation cores. For instance, the structure labeled with $\Sigma = 193$, p1p11 shown in Fig. 4(h) has the primary 5-7 pair followed by one hexagon, followed by the secondary 5-7 pair and 11 hexagons. The sum of hexagons and nonhexagonal rings due to the 5-7 pairs per period d needs to sum up to n_{rings}, so that the total number of hexagons per period in the grain boundary is determined by

$$n_{n=6} = n_{\text{rings}} - 2n_d = 3m - n, \tag{14}$$

and each section of hexagons needs to have an odd number of rings to form a straight grain-boundary line. The grain-boundary structure that has the most equally separated primary and secondary dislocation arrays is the p5p7 structure in Fig. 4(i), which would be expected to be the lowest-energy configuration for the $\Sigma = 193$ grain boundary. Figure 6, however, shows that the structures with lowest energy for the $\Sigma = 193$ grain boundary are actually the p1p11. As shown in Fig. 6, also for all other members of the $n_d = 2$ family, the lowest-energy configurations are those where the dislocation cores in the primary and secondary dislocation arrays are as close as possible to each other. This indicates that the dislocation cores in graphene actually attract each other, in contrast to dislocation cores in three-dimensional materials.

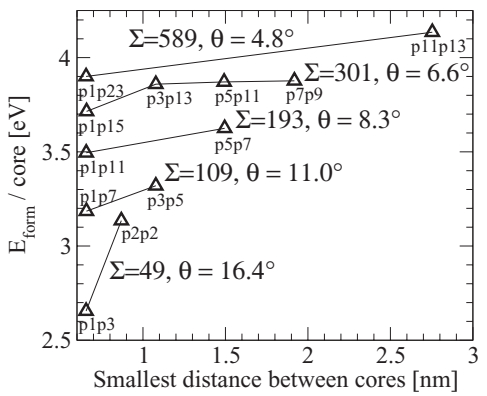

FIG. 6. Formation energy E_{form} for different separations between the primary and secondary dislocation cores in the grain boundaries belonging to the $n_d = 2$ family.

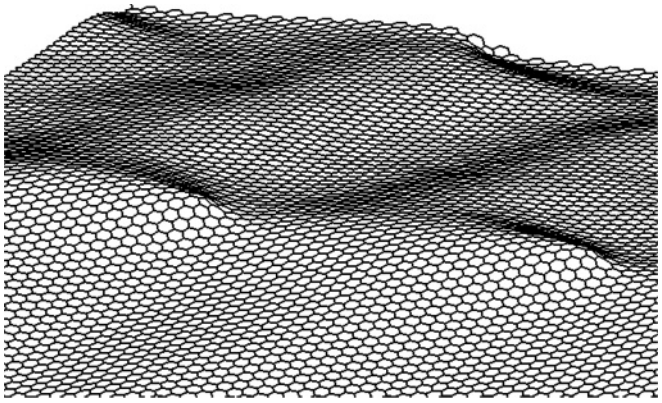

FIG. 7. View of the fully relaxed $\Sigma = 721$ grain boundary, which has the shape of an array of asymmetric hillocks similar to those observed by STM in Ref. 18.

The attraction between the dislocation cores occurs because they form hillocks as can be seen in Figs. 4 and 7. The two-dimensional nature of graphene allows for buckling of the sheet, so that the strain induced by the 5-7 pairs can partly be released by bending the graphene sheet out of plane to form a hillock around the dislocation core. The strain energy around each dislocation core is further diminished by moving the dislocation cores closer to each other since they form a larger hillock that contains more than one dislocation core and has smaller curvature and, consequently, less strain.

The formation of the hillocks at the grain boundary has been discussed in some of the recent theoretical papers[23,26] and it is in good agreement with the STM observation of a low-misorientation-angle grain boundary in graphene grown on Ir(111).[18] In Ref. 18, the authors found that the grain boundary formed an array of asymmetric hillocks and that each hillock contained one dislocation core. The separation between the hillocks was estimated to be ∼62 nm and the misorientation angle to 2.07°. We can use Eq. (9) to find the CSL grain boundary that is the closest match to this observation. Since the grain boundary was reported to be a periodic array of hillocks, we can assume that the observed grain boundary belongs to the family $n_d = 1$. Using the measured values gives $\Sigma \approx 766$, which is not an exact CSL grain boundary, so that the $\Sigma = 721$ [0001] tilt grain boundary is the closest match, with $\theta = 2.13°$ and period $d = 66$ nm. The calculated structure of the $\Sigma = 721$ grain boundary in Fig. 7 shows a nonsymmetric hillock structure, very similar to the STM pictures in Ref. 18. The hillock height is 3.21 Å (see also Fig. 8).

The same mechanism of strain reduction that leads to attractions between dislocation cores applies to grain boundaries with larger misorientation angles, where the dislocation cores get closer and closer according to Frank's formula [Eq. (5)]. In Fig. 8, we show (upper panel) the height variation along the grain boundary and (lower panel) the much larger variation in the direction perpendicular to it. For graphene on a substrate, the latter is suppressed, whereas the height variation along the grain boundary should not change. In the upper panel, the behavior of the out-of-plane variation is very smooth within the families $n_d = 1$ and $n_d = 2$. For $n_d = 3$, there is some scattering that is probably related to the fact that, in the presence of several secondary dislocation cores, it is

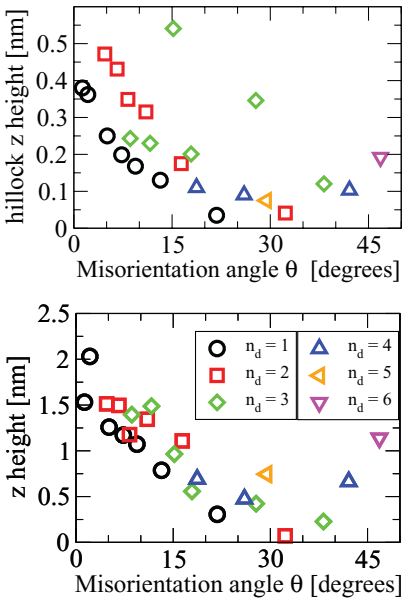

FIG. 8. (Color online) Out-of-plane variation along (upper panel) and perpendicular to (lower panel) the grain boundary as a function of the misorientation angle θ.

difficult to find the absolute minimum structure. Possibly, more sophisticated schemes of structural minimization should be used for these cases, such as for complex clusters.[35] In Fig. 8 (upper panel), it can be seen that the pronounced height variation of the hillocks at small misorientation angles decreases and becomes close to zero between 20° and 40°. This can be understood because, in this range, the misorientation angle approaches the *ideal* dislocation angle $\theta_d = 180/7 \approx 25°$, which is defined as the misorientation angle that the lattice needs to be opened to insert one additional lattice plane to form an edge dislocation. The grain boundaries that have a misorientation angle close to θ_d experience only a small strain due to the dislocation cores. These grain boundaries remain flat as the strain is not strong enough to push the dislocation cores out of the plane of the graphene sheet. In addition, the dislocation cores may come so close that the grain-boundary region is completely covered by nonhexagonal rings. Equation (14) reveals that the grain-boundary region contains no hexagons and only pentagons and heptagons if $n = 3m$. Our calculations show that the $\Sigma = 13$ grain boundary that has $(m,n) = (1,3)$ indeed only contains pentagons and heptagons (and no hexagons), as can be seen in Fig. 4(g). The misorientation angle $\theta = 32.2°$ of the $\Sigma = 13$ grain boundary consequently defines a limiting misorientation angle. Grain boundaries with a larger misorientation angle $\theta > 32.2°$ have such a high density of pentagons and heptagons that they become faceted and contain zigzag arrays of dislocation cores. The very recent observation of faceted grain boundaries[13] may be interpreted in this way.

C. Formation energies

The gradual variation of the structure depending on the misorientation angle is also reflected in the formation energy of the [0001] tilt grain boundaries, as can be seen in Fig. 5. As discussed in Sec. III, all three methods used to calculate the formation energies are in qualitative agreement. However, the values calculated with the Dreiding force field are overestimated compared to the DFT values. This is due to the fact that the spring constant of the Dreiding force field is approximately 1.5 times too stiff compared to *ab initio* values. The values calculated with the LCBOPII force field instead agree very well with the DFT values, so that we are confident that the formation energies calculated with LCBOPII for smaller misorientation angles that require very large supercells are reliable.

The formation energies per unit length in Fig. 5 increase smoothly for small θ, and the formation energy curve starts to bend over at $\theta > 10°$ and reaches a maximum at $\theta \approx 28°$. Interestingly, the formation energies in Fig. 5 follow a single line irrespective of which family the grain boundary belongs to. This shows that graphene is so flexible that the secondary dislocation arrays do not cause more strain than the primary dislocation array, as is often the case in three-dimensional materials.[31] However, the $\Sigma = 13$ grain boundary has a particularly low formation energy that provides a secondary minimum at $\theta = 32.2°$, in agreement with previous calculations.[23,26] The low formation energy of the $\Sigma = 13$ grain boundary is also in agreement with the particularly high yield strength for this grain boundary, which was observed in molecular dynamics calculations of grain boundaries in graphene under stress .[14]

We have found that a more insightful representation of the formation energy is given by looking at the formation energy *per dislocation core* rather than to the formation energy per unit length, as is customary. In Fig. 9, we show that the formation energy per dislocation core displays two different behaviors, a logarithmic decay for small misorientation angles and a linear decay for larger misorientation angles leading to a V shape around $\theta = 32.2°$.

In the treatment of grain boundaries in bulk three-dimensional materials, it has been proposed by Koehler[36]

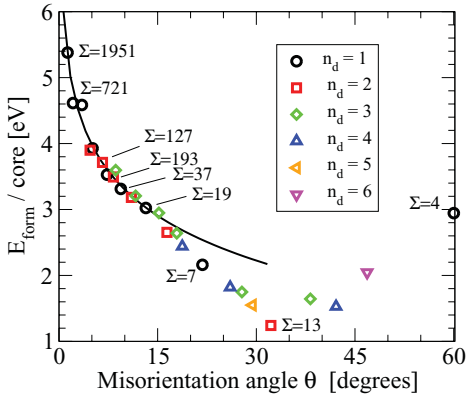

FIG. 9. (Color online) The formation energy per dislocation core as a function of the misorientation angle θ calculated with LCBOPII (open circles). The continuous curve is the fit to the data with Eq. (17). Only the data for misorientation angles smaller than 10° are used to fit the curve, which is then prolonged up to $\theta = 32.2°$. Notice that the V shape of this curve resembles that of the out-of-plane distortions shown in Fig. 8.

and Read-Shokley[21] to divide the formation energy into two parts

$$E_{\text{form}} = E_{\text{core}} + E_{\text{strain}}, \tag{15}$$

namely, a constant term E_{core} due to the local distortions of the bond angles and change in hybridization at the 5-ring and 7-ring in the dislocation core with respect to the bulk hexagonal lattice and a term E_{strain} due to the deformation of the graphene lattice away from the dislocation cores. For small misorientation angles, where the dislocation cores have a separation much larger than interatomic distances and the core-core interaction is negligible, the formation energy can be estimated by the Read-Shockley equation[21] for the formation energy per unit length as:

$$E_{\text{form}}^{R-S} = \theta A \left[B - \ln(\theta)\right], \tag{16}$$

where A and B are constants depending on electronic and elastic properties of the material. We can express the formation energy per dislocation core by dividing Eq. (16) by the number of dislocation cores per unit length. The latter quantity is equal, for small misorientation angles, to θ/a. Indeed, the number of dislocation cores per unit length is $n_d/d = b/(ad)$. Considering that $\theta = b/d$, it follows that $n_d/d = \theta/a$. The formation energy per dislocation core is then

$$E_{\text{form}} = C - D\ln(\theta). \tag{17}$$

We note that the above expressions are dimensionally correct for a 2D crystal. For a 3D crystal, there would be an extra linear dimension so that Eq. (16) would express an energy per unit area and Eq. (17) an energy per dislocation core per unit length. Furthermore, in the 3D case, the parameter A can be directly related to the bulk elastic shear modulus and the Poisson's ratio of the material;[21] in the 2D case, this is not easily achievable due to the important role played by the large (i.e., nonharmonic) out-of-plane displacements, which are not described by the in-plane elastic constants.

We fit the formation energy per dislocation core of Fig. 9 with the functional form of Eq. (17), keeping C and D as fit parameters, yielding $C = 1.59$ eV/core and $D = 0.98$ eV/core. In Fig. 9, we show the fitted curve up to $\theta = 32.2^\circ$. The value of the fitting parameter C can be interpreted as the dislocation core energy E_{core}. Our estimate is a value much smaller than in Ref. 23, where the formation energy per dislocation core is erroneously taken as the slope at small misorientation angles of the energy per unit length curve. In fact, such a curve has infinite derivative for θ going to zero. The dislocation core energy found by our fit to the small-misorientation-angle data can be compared to the difference in heat of formation between the naphthalene (two hexagons) and the azulene (one pentagon and one heptagon) molecules ΔH_{form}, for which our DFT calculations give $\Delta H_{\text{form}} = 1.4$ eV. In Fig. 9, we show the result of the fit at small misorientation angles of the formation energy per dislocation core as a solid line. We see that this form describes very well our data in the limit of small misorientation angles and up to $\theta \sim 12^\circ$, not only for the $n_d = 1$ family, but for all studied cases. At larger misorientation angles, the logarithmic decay of the formation energy predicted by the Read-Shockley equation does not apply anymore and the deviation of the calculated formation energies toward lower values can be connected to the dislocation core interaction, which is neglected in the Read-Shockley equation. As already argued, in graphene, the core-core interaction is always negative and dislocation cores always attract each other. In fact, the dislocation cores form hillocks that relieve the in-plane strain and the dislocation cores interact via these hillocks. Increasing the misorientation angle decreases the strain that the dislocation cores induce, which is reflected in smaller out-of-plane distortion and lower formation energies than predicted by the Read-Shockley equation. Comparing the formation energies in Fig. 9 to the magnitude of the out-of-plane distortion in Fig. 8 shows a very good correlation, indicating that the dislocation cores induce a large strain in small-misorientation-angle grain boundaries, which leads to a large out-of-plane distortion and a large formation energy. By increasing the misorientation angle, the hillocks gradually coalescence into flat ridges along the grain boundary and the strain is largely reduced. The formation energies calculated by LCBOPII are lower than the values predicted by the Read-Schockley equation in this regime, and the decay of the formation energies is linear rather than logarithmic. For still larger misorientation angles around the ideal dislocation angle θ_d, the dislocation cores fit into the lattice almost perfectly, and the grain-boundary region becomes almost flat for the $\Sigma = 13$ grain boundary where the formation energy per dislocation cores reaches an absolute minimum.

In summary, the results for grain boundaries in a two-dimensional material such as graphene reveal a number of aspects that are different from those of grain boundaries in three-dimensional bulk materials since the dislocation cores have the freedom to move out of plane to relieve strain, yielding an effective core-core attraction.

V. SUMMARY AND CONCLUSIONS

We have developed a general theory for the structure of [0001] tilt grain boundaries in graphene based on the coincidence site lattice (CSL) method. The theory provides expressions for the misorientation angle θ, periodicity d, Burger's vector b, and the size of the unit cell Σ for the grain boundaries in graphene in terms of the grain-boundary indices (m,n). Our force field and DFT calculations show that low energy grain boundaries with misorientation angles $\leqslant 32.2^\circ$ can be identified as dislocation arrays. Grain boundaries with misorientation angles larger than 32.2° can also have other nonhexagonal rings in the grain boundary region. Small-misorientation-angle grain boundaries tend to form hillocks due to the strain at the dislocation cores in agreement with STM observations of small-misorientation-angle grain boundaries, epitaxial grown graphene, and in HOPG. We have shown that, contrary to the usual bulk behavior, in graphene there is an attractive interaction between dislocation cores that decreases the strain energy, so that the dislocation arrays form ridges for misorientation angles $10^\circ < \theta < 25^\circ$ and flatten out for misorientation angles around $\theta = 32.2^\circ$. This interaction decreases the formation energy for grain boundaries with large misorientation angles so that a minimum occurs for $\Sigma = 13$ at $\theta = 32.2^\circ$. We discussed a large number

of grain boundaries that are relevant for the discussion of the experimental observations up to now. The use of an accurate reactive potential has allowed us to describe in detail also grain boundaries that have long period. We have pointed out the crucial role of out-of-plane distortion for achieving the minimal energy structures, a feature that is crucial for the description of grain boundaries in two-dimensional materials.

ACKNOWLEDGMENTS

The authors acknowledge M. Scheffler for a critical reading of the manuscript and thank P. Bristowe for fruitful discussions. A.F. acknowledges support of the Stichting voor Fundamenteel Onderzoek der Materie (FOM), which is financially supported by the Nederlandse Organisatie voor Wetenschappelijk Onderzoek (NWO) and thanks M. A. Akhukov, J. H. Los, and M. I. Katsnelson for useful discussions.

*jcarlsson@accelrys.com

[1] K. S. Novoselov, A. K. Geim, S. V. Morozov, D. Jiang, Y. Zhang, S. V. Dubonos, I. V. Grigorieva, and A. A. Firsov, Science **306**, 666 (2004).

[2] M. I. Katsnelson, K. S. Novoselov, and A. K. Geim, Nat. Phys. **2**, 620 (2006).

[3] J. C. Meyer, A. K. Geim, M. I. Katsnelson, K. S. Novoselov, T. J. Booth, and S. Roth, Nature (London) **446**, 60 (2007).

[4] K. V. Zakharchenko, M. I. Katsnelson, and A. Fasolino, Phys. Rev. Lett. **102**, 046808 (2009).

[5] T. J. Booth, P. Blake, R. R. Nair, D. Jiang, E. W. Hill, U. Bangert, A. Bleloch, M. Gass, K. S. Novoselov, M. I. Katsnelson, and A. K. Geim, Nano Letters **8**, 2442 (2008).

[6] C. Lee, X. Wei, J. W. Kysar, and J. Hone, Science **321**, 385 (2008).

[7] C. Berger, Z. Song, X. Li, X. Wu, N. Brown, C. Naud, D. Mayou, T. Li, J. Hass, A. N. Marchenkov, E. H. Conrad, P. N. First, and W. A. de Heer, Science **312**, 1191 (2006).

[8] K. V. Emtsev, A. Bostwick, K. Horn, J. Jobst, G. L. Kellogg, L. Ley, J. L. McChesney, T. Ohta, S. A. Reshanov, J. Röhrl, E. Rotenberg, A. K. Schmid, D. Waldmann, H. B. Weber, and T. Seyller, Nat. Mater. **8**, 203 (2009).

[9] K. S. Kim, Y. Zhao, H. Jang, S. Yoon Lee, J. M. Kim, K. S. Kim, J.-H. Ahn, P. Kim, J.-Y. Choi, and B. H. Hong, Nature (London) **457**, 706 (2009).

[10] A. Reina, X. T. Jia, J. Ho, D. Nezich, H. B. Son, V. Bulovic, M. S. Dresselhaus, and J. Kong, Nano Lett. **9**, 30 (2009).

[11] Q. Yu, J. Lian, S. Siriponglert, H. Li, Y. P. Chen, and S.-S. Pei, Appl. Phys. Lett. **93**, 113103 (2008).

[12] X. Li, W. Cai, J. An, S. Kim, J. Nah, D. Yang, R. Piner, A. Velamakanni, I. Jung, E. Tutuc, S. K. Banerjee, L. Colombo, and R. S. Ruoff, Science **324**, 1312 (2009).

[13] P. Y. Huang, P. Y. Huang, C. S. Ruiz-Vargas, A. M. van der Zande, W. S. Whitney, M. P. Levendorf, J. W. Kevek, S. Garg, J. S. Alden, C. J. Hustedt, Y. Zhu, J. Park, P. L. McEuen, and D. A. Muller, Nature (London) **469**, 389 (2011).

[14] R. Grantab, V. B. Shenoy, and R. S. Ruoff, Science **330**, 946 (2010).

[15] J. Lahiri, Y. Lin, P. Bozkurt, I. I. Oleynik, and M. Batzhill, Nat. Nanotechnol. **5**, 326 (2010).

[16] D. Gunlycke and C. T. White, Phys. Rev. Lett. **106**, 136806 (2011).

[17] T. R. Albrecht, H. A. Mizes, J. Nogami, S.-I. Park, and C. F. Quate, Appl. Phys. Lett. **52**, 362 (1988).

[18] J. Coraux, A. T. N'Diaye, C. Busse, and T. Michely, Nano Lett. **8**, 565 (2008).

[19] P. Simonis, C. Goffaux, P. A. Thiry, L. P. Biro, P. Lambin, and V. Meunier, Surf. Sci. **511**, 319 (2002).

[20] J. Cervenka and C. F. J. Flipse, Phys. Rev. B **79**, 195429 (2009).

[21] W. T. Read and W. Shockley, Phys. Rev. **78**, 275 (1950).

[22] A. Sutton and V. Vitek, Philos. Trans. R. Soc. A **309**, 1 (1983).

[23] O. V. Yazyev and S. G. Louie, Phys. Rev. B **81**, 195420 (2010).

[24] Y. Liu and B. Yakobson, Nano Lett. **10**, 2178 (2010).

[25] O. V. Yazyev and S. G. Louie, Nat. Mater. **9**, 806 (2010).

[26] T.-H. Liu, G. Gajewski, C.-W. Pao, and C.-C. Chang, Carbon **49**, 2306 (2011).

[27] S. Malola, H. Häkkinen, and P. Koskinen, Phys. Rev. B **81**, 165447 (2010).

[28] A. Mesaros, S. Papanikolaou, C. F. J. Flipse, D. Sadri, and J. Zaanen, Phys. Rev. B **82**, 205119 (2010).

[29] S. Mayo, B. D. Olafson, and W. A. Goddard III, J. Chem. Phys. **94**, 8897 (1990).

[30] J. H. Los, L. M. Ghiringhelli, E. J. Meijer, and A. Fasolino, Phys. Rev. B **72**, 214102 (2005).

[31] A. Sutton and R. W. Baluffi, *Interfaces in Crystalline Materials* (Oxford University Press, Oxford, UK, 1995).

[32] Materials Studio release 5.5, Accelrys Software Inc., San Diego, USA (2010).

[33] J. P. Perdew, K. Burke, and M. Ernzerhof, Phys. Rev. Lett. **77**, 3865 (1996).

[34] The CASTEP code: S. J. Clark, M. D. Segall, C. J. Pickard, P. J. Hasnip, M. J. Probert, K. Refson, and M. Payne, Z. Kristallogr. **220**, 567 (2005).

[35] D. M. Deaven and K. M. Ho, Phys. Rev. Lett. **75**, 288 (1995).

[36] J. S. Koehler, Phys. Rev. **60**, 397 (1941).